

Ponderomotive coupling of waves to sea surface currents via horizontal density gradients

Darryl D. Holm, Ruiao Hu and Oliver D. Street*

d.holm@imperial.ac.uk, ruiao.hu15@imperial.ac.uk, o.street18@imperial.ac.uk

Department of Mathematics, Imperial College London
SW7 2AZ, London, UK

Key words: nonlinear water waves, free surface fluid dynamics, geometric mechanics

Abstract

The mathematical models and numerical simulations reported here are motivated by satellite observations of horizontal sea surface fluid motions that are closely coordinated with the vertical motion of waves or, after an approximation, an envelope of rapidly oscillating waves. This coordination of fluid movements with wave envelopes tends to occur when strong horizontal buoyancy gradients are present. The nonlinear models of this coordinated movement presented here may provide future opportunities for the optimal design of satellite imagery that could simultaneously capture the dynamics of both waves and currents directly.

The models derived here appear first in their unapproximated form, then again with a slowly varying envelope (SVE) approximation using the WKB approach. The WKB wave-current-buoyancy interaction model derived here for a free surface with horizontal buoyancy gradients indicates that the mechanism for these correlations is the ponderomotive force of the slowly varying envelope of rapidly oscillating waves acting on the surface currents via the horizontal buoyancy gradient. In this model, the buoyancy gradient appears explicitly in the WKB wave momentum, which in turn generates density-weighted potential vorticity whenever the buoyancy gradient is not aligned with the wave-envelope gradient.

Contents

1	Introduction	1
1.1	Submesoscale sea surface dynamics	1
2	Submesoscale thermal wave-current dynamics	3
2.1	A tale of two maps: currents and waves	3
2.2	Thermal potential vorticity (TPV) dynamics	8
2.3	WCIFS equations in the SVE approximation	10
2.4	Thermal potential vorticity dynamics with SVE	12
3	Numerical implementation	13
4	Conclusion and Outlook	15

1 Introduction

1.1 Submesoscale sea surface dynamics

Capabilities in sea surface observation are now burgeoning. The new high-resolution satellite observation capabilities are revealing submesoscale sea surface features at spatial scales of 100 m –

*Corresponding author, email: o.street18@imperial.ac.uk

10 km and time scales of hours to weeks. Invariably, the new satellite imagery reveals a plethora of coupled dynamical phenomena, including currents, spiral filaments, flotsam patterns, jets and fronts, some of which are detected indirectly through sea surface temperature, salinity or colour, in addition to the imagery [3, 8, 11].

For example, the impending Surface Water Ocean Topography (SWOT) mission will map the ocean surface mesoscale sea surface height field, as well as a large fraction of the associated submesoscale field, including buoyancy fronts [15]. A sample of this type of submesoscale data taken from [3] is shown in figures 1 and 2. The new age of high-resolution upper ocean observations will present a formidable array of challenges for the next generation of computational mathematics and numerical simulations. Meeting these challenges will require a principle-based strategy for deterministic modelling, as well as uncertainty quantification through stochastic modelling and mathematical analysis, applied in concert with high-resolution observations, computational simulations, and stochastic data assimilation for large data sets.

These higher-quality observations raise challenges in data management, computational simulation and mathematical modelling. One challenge involves the upper ocean's response to increased atmospheric climate warming. Namely, how does the increased atmospheric heating influence the dynamics of the ocean surface? How does one predict the effects of the stronger thermal fronts and 'marine heat waves' that are expected to develop? In short, the question is how much will thermal fronts and their associated buoyancy gradients perturb the dynamics of the ocean's wave and currents [17]?

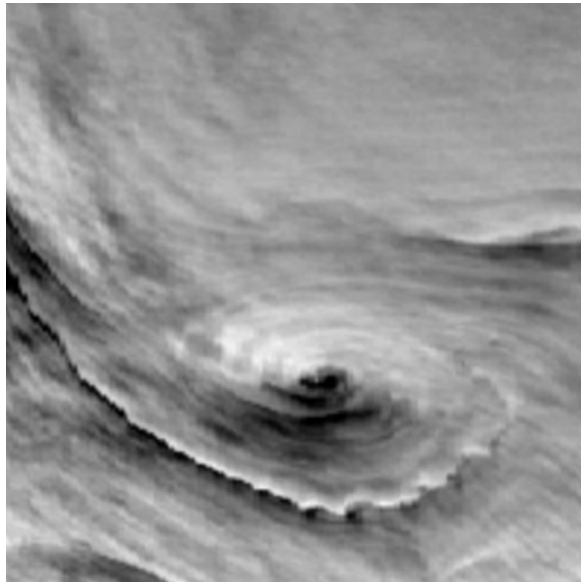
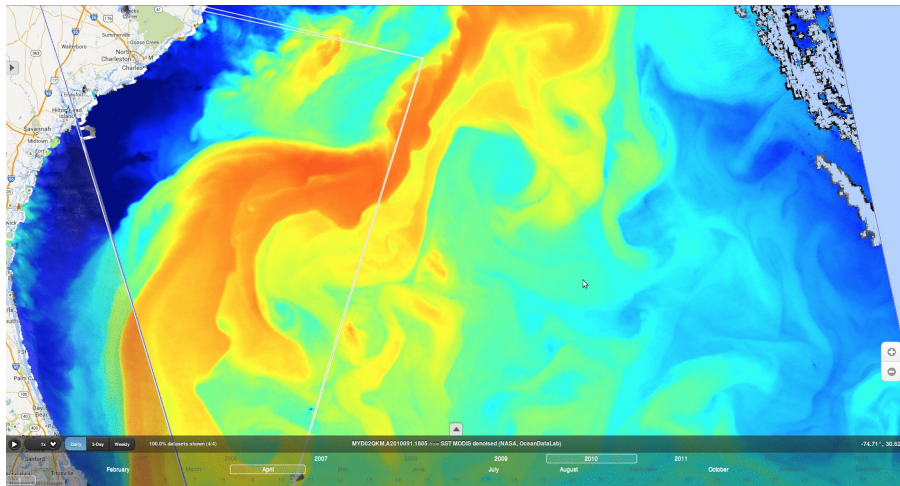
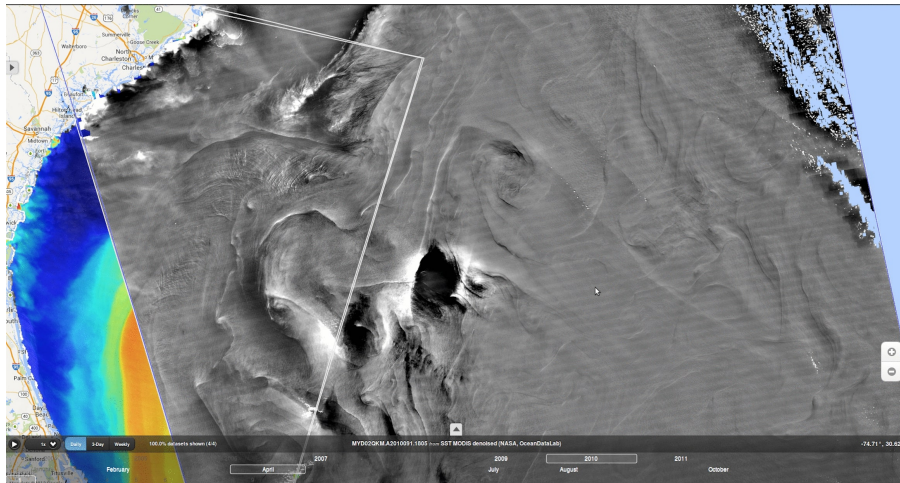


Figure 1: Wave activity in the submesoscale ocean is dynamically complex, as illustrated in this figure showing the zoomed image of a submesoscale sea surface elevation, seen in Envisat MERIS glitter observations. This image shows the wave elevation tracking a cyclonic eddy visible in the sea surface glitter observations. The pixel resolution is 250m. This glitter image demonstrates the complex, highly-coordinated dynamical forms taken in wave-current interaction on the submesoscale sea surface. In particular, notice the instabilities developing in the eddy's outer boundary. Image courtesy of B. Chapron.

Emergent coherence (EC). Combining high-resolution thermal data (buoyancy) with glitter data for the wave elevation as in figure 2 has recently revealed another interesting feature of submesoscale dynamics. Namely, the observed submesoscale data show extremely high correlations of wave, current and thermal properties [3]. This emergent spatial-temporal coherence of dynamic and thermal properties presents a significant challenge for dynamical submesoscale modelling. Accepting this challenge, the aim of this paper is to derive a mathematical model of nonlinear sea surface dynamics whose solutions also demonstrate the emergent coherence observed in combining different types of submesoscale data. This paper derives new equations that show the emergent



(a) Sea surface temperature near the Gulf Stream, on April 1st 2010, from the Envisat AATSR measurements.



(b) Sea surface glitter contrasts near the Gulf Stream, on April 1st 2010, from the Envisat MERIS observations.

Figure 2: Comparison of the two images above demonstrates the emergent coherence between sea surface temperature and the glitter patterns visible from satellite imagery. The thermal fronts visible are dynamic, and sea surface roughness is most obvious along the strongest fronts. Images courtesy of B. Chapron.

coherence (EC) seen in figure 2. The EC behaviour produced by the equations are demonstrated in figure 3 which shows a snapshot of the coherence of buoyancy and wave amplitude distributions in the dynamics of divergence-free flow on a free surface moving under gravity. In the model equations the horizontal buoyancy gradients mediate the interactions between the waves and currents.

2 Submesoscale thermal wave-current dynamics on a free surface

2.1 A tale of two maps: currents and waves

Waves on the surface of the ocean are modelled here as a composition of two smooth invertible maps describing the temporal evolution and advection of two degrees of dynamical freedom interacting at widely separated space-time scales. In this composition of maps, the waves are regarded as local vertical disturbances that rapidly oscillate as they are swept along by the broad, slowly changing horizontal currents. Thus, the slow current motion is a Lagrangian coordinate for the rapid wave oscillations. This wide separation in space-time scales invokes the classical WKB description. The standard WKB approach seeks a rapidly oscillating wave packet solution whose phase-averaged

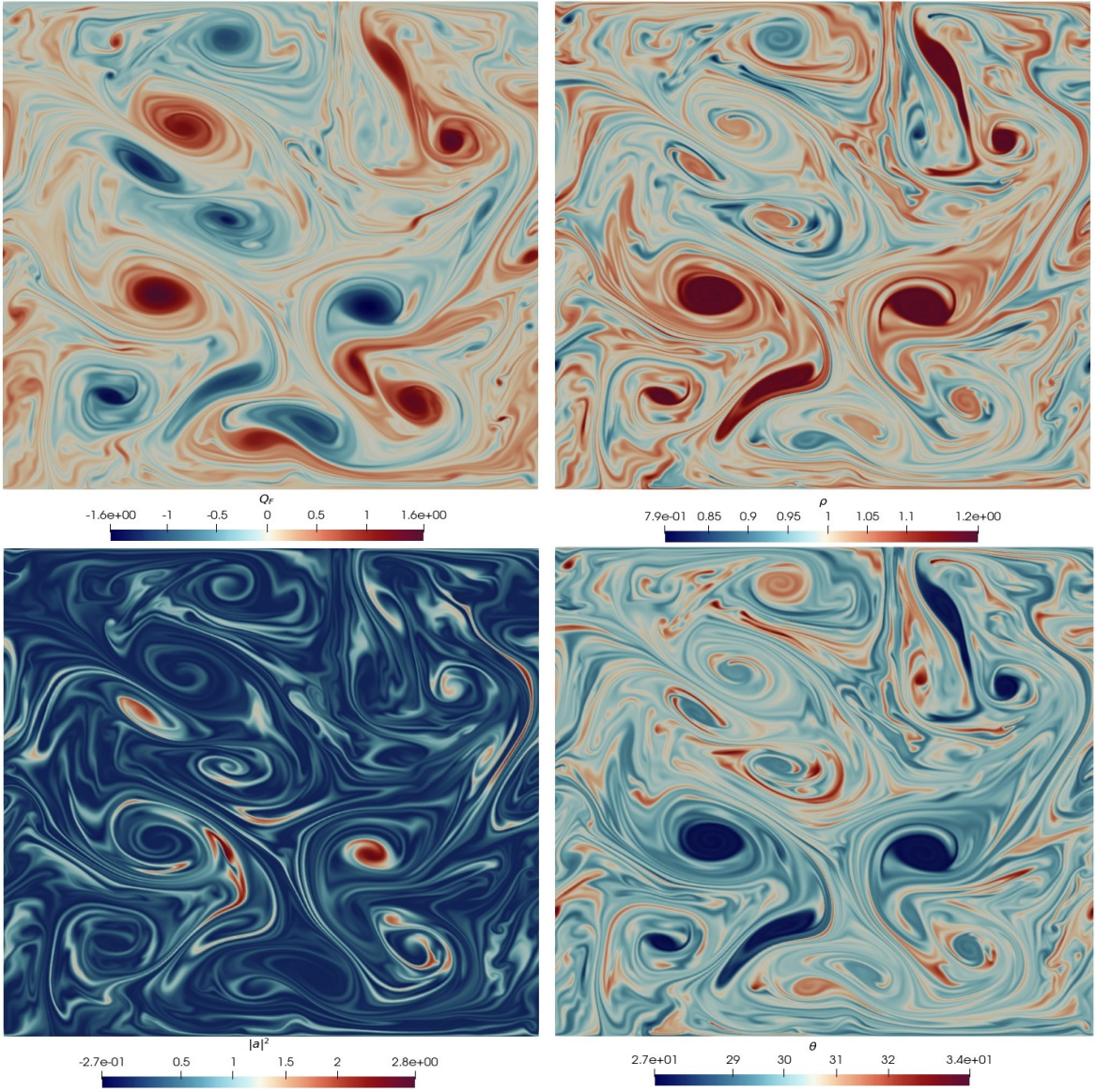


Figure 3: This is a 512^2 snapshot of the WCIFS equations in the SVE approximation in the potential vorticity form in (2.41). The four panels display the following distributions, modified potential vorticity Q -PV in (2.39) (top left), buoyancy (top right), square of the wave amplitude (bottom left) and wave phase (bottom right) in the numerical simulation of the dynamics of divergence-free flow on a free surface moving under gravity. The simulation began with a spin-up period with zero wave amplitude. After the spin-up period, as explained in section 3, a checker-board pattern of finite wave amplitude with *zero phase* was introduced and the simulation was resumed. The ‘mixing’ of these wave patterns eventually brought them into coherence with the spatial distributions of thermal properties and potential vorticity. These features show an emergent coherence in patterns similar to those seen in the corresponding high-resolution satellite data in figure 2.

amplitude possesses a slowly varying envelope (SVE) spatially. The WKB method is often applied via a variational principle because in a variational setting the phase average naturally leads to an adiabatic invariant known as the wave action density, cf. for example, [1] for a review of the WKB or SVE method in fluid dynamics. Here we will follow the variational approach of [2, 9] guided by the classical work of [19, 21, 22].

The position and velocity of fluid parcels in motion under gravity on a 2D free surface embedded in \mathbb{R}^3 have both horizontal and vertical components. The corresponding flow maps are denoted as the map $\phi_t : \mathbb{R}^2 \rightarrow \mathbb{R}^2$ for the horizontal current flow, and as the composite map $\zeta_t \phi_t$ for the vertical elevation of the waves as a function of time and position in \mathbb{R}^2 . The flow lines of these two components

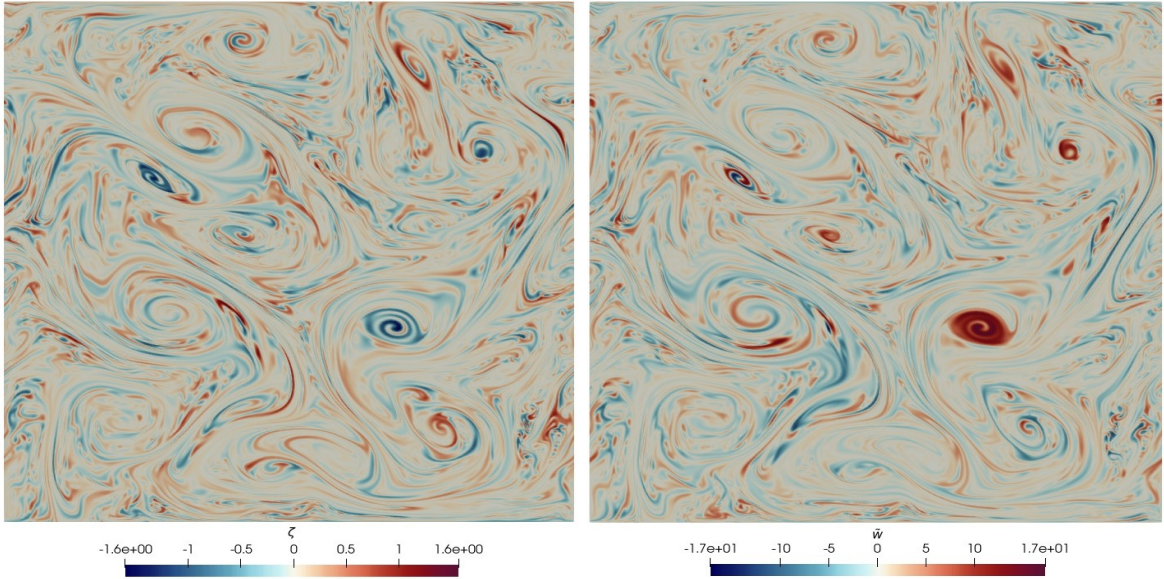


Figure 4: These 512^2 snapshots of the WCIFS simulation in the vorticity form (2.21) shows the elevation ζ in the left panel and the density-weighted vertical velocity \tilde{w} on the right. The snapshots are taken at the same time and with the same fluid spin-up initial conditions as the snapshots of the simulation of the SVE approximate equations presented in Figure 3. Overlaying the two figures demonstrates that the resolved features in the ζ distribution in this figure of WCIFS results are bounded by the SVE wave envelope distribution $|a|^2$ in Figure 3.

of the flow map of a free surface can be written as

$$\mathbf{r}_t = \phi_t \mathbf{r}_0 \quad \text{and} \quad z_t = \zeta_t(\phi_t \mathbf{r}_0) =: \zeta_t(\mathbf{r}_t),$$

where $\mathbf{r}_t = (x_t, y_t) \in \mathbb{R}^2$ is the horizontal position along the flow at time t and $\zeta_t(\mathbf{r}_t)$ is the vertical elevation at horizontal position \mathbf{r}_t at time t , starting at position \mathbf{r}_0 at time $t = 0$. Thus, one may say that the initial position of the flow line, \mathbf{r}_0 , is a Lagrangian coordinate for the horizontal motion, and the horizontal motion is a Lagrangian coordinate for the vertical motion. That is, the ‘footpoint’ at time t of the vertical component of the flow map ζ_t is located in the horizontal plane along a curve $\phi_t \mathbf{r}_0$ parameterised by time t . Likewise, one can simply say that the wave dynamics is advected, or swept along, by the current dynamics.

Hence, the corresponding horizontal and vertical components of velocity along a stream line \mathbf{r}_t in the horizontal plane are defined by,

$$\begin{aligned} \frac{d\mathbf{r}_t}{dt} &= \frac{d}{dt}(\phi_t \mathbf{r}_0) = \hat{\mathbf{v}}_t(\phi_t \mathbf{r}_0) =: \hat{\mathbf{v}}_t(\mathbf{r}_t), \quad \text{so} \quad \hat{\mathbf{v}}_t = \frac{d\phi_t}{dt} \phi_t^{-1} \quad \text{and} \\ \frac{dz_t}{dt} &=: \hat{w}_t(\mathbf{r}_t) = \frac{d}{dt}(\zeta_t(\phi_t \mathbf{r}_0)) = \partial_t \zeta_t(\mathbf{r}_t) + \nabla_{\mathbf{r}} \zeta_t(\mathbf{r}_t) \cdot \hat{\mathbf{v}}_t(\mathbf{r}_t). \end{aligned}$$

That is, in the dynamics of free surface flow, the vertical velocity $\hat{w}(\mathbf{r}, t)$ at a given Eulerian point \mathbf{r} and time t is related to the wave elevation $\zeta(\mathbf{r}, t)$ and horizontal velocity $\hat{\mathbf{v}}(\mathbf{r}, t)$ at that point by

$$\hat{w}(\mathbf{r}, t) = \partial_t \zeta(\mathbf{r}, t) + \hat{\mathbf{v}}(\mathbf{r}, t) \cdot \nabla_{\mathbf{r}} \zeta(\mathbf{r}, t).$$

In terms of these fluid variables, Hamilton’s principle for wave-current interaction of a free surface is obtained by following [6] for the variational modelling framework and [21, 5] for the potential energy

to find¹

$$\begin{aligned} 0 = \delta S &= \delta \int_a^b \ell(\hat{\mathbf{v}}, \zeta, D, \rho) dt \\ &= \delta \int_a^b \int_{\mathcal{D}} \left(\frac{1}{2} \left(|\hat{\mathbf{v}}|^2 + \sigma^2 (\partial_t \zeta + \nabla_{\mathbf{r}} \zeta \cdot \hat{\mathbf{v}})^2 \right) - \frac{\zeta^2}{2Fr^2} \right) D\rho - p(D-1) d^2r dt. \end{aligned} \quad (2.1)$$

Estimating parameters σ^2 and Fr^2 for satellite observations. The Lagrangian $\ell(\hat{\mathbf{v}}, \zeta, D, \rho)$ in (2.1) represents the dimension-free difference of the kinetic and potential energies, augmented by the incompressibility constraint imposed by the Lagrange multiplier p . Two dimension-free parameters (σ^2 and Fr^2) appear in this Hamilton's principle. The coefficient $\sigma^2 = ([H]/[L])^2$ in formula (2.1) is the square of the vertical-to-horizontal aspect ratio. Typically, for satellite observations of submesoscale dynamics one finds

$$[H] \approx (3 \times 10^{-4} - 3 \times 10^{-3}) km \quad \text{and} \quad [L] \approx (10^{-1} - 10) km, \quad \text{so} \quad \sigma^2 \approx 10^{-3} - 10^{-6} \ll 1$$

for the squared aspect ratio $\sigma^2 \ll 1$ of the height of the waves $[H]$ relative to the breadth $[L]$ of the two-dimensional domain. The squared Froude number Fr^2 in this regime is estimated by

$$Fr^2 := \left(\frac{[V]}{N[H]} \right)^2 \approx 1 - 10^4 \quad \text{and} \quad \sigma^2 = ([H]/[L])^2 \approx 10^{-3} - 10^{-6} \quad (2.2)$$

for horizontal velocity $[V] = (10^{-1} - 1) m/sec$, $[H] = (3 \times 10^{-1} - 3) m$, and Brunt-Väisälä buoyancy frequency $N \approx (10^{-3} - 10^{-4})/sec$ in the submesoscale mix layer (SML) [7]. Hence, we estimate that the squared product of the Froude number and aspect ratio for satellite observations can reasonably be estimated over the range

$$\sigma^2 Fr^2 := \left(\frac{[V]}{N[L]} \right)^2 \approx 10^{-3} - 10. \quad (2.3)$$

Modelling the dynamic effects of surface density variations. Let us say a few words about how one models the dynamic effects of surface density variations on the wave properties in the non-dimensional form of Hamilton's principle in (2.1). As one might have expected, numerical simulations of the equations resulting from the Hamilton's principle in (2.1) show that multiplying both the kinetic energy and the potential energy of the waves by the same space and time dependent surface density ρ tends to synchronise the wave oscillations throughout the domain. However, the observed oscillations of the waves are by no means simultaneous across the whole domain, although they are indeed coordinated spatially with the buoyancy of the fluid. To correct this solution behaviour, the kinetic energy and potential energy need to be de-synchronised from the buoyancy.

The dynamic dependence of the wave kinetic energy on the density is physically required. However, to de-synchronise the wave oscillations we can introduce a constant reference density ρ_{ref} into the wave potential energy, by writing

$$\frac{\zeta^2}{Fr^2} \rightarrow \frac{\rho_{ref}}{\rho} \frac{\zeta^2}{Fr^2} \quad \text{with} \quad \frac{\rho_{ref}}{\rho} \quad \text{of order} \quad O(1). \quad (2.4)$$

The quantity ρ_{ref} is a constant reference density, and the density ratio $(\rho_{ref}/\rho) = O(1)$

The density dependence imposed here is important in the dynamics that follows from Hamilton's principle. Substituting the relations in (2.4) into Hamilton's principle in equation (2.1) leads to the following dimension-free action integral,

$$\begin{aligned} 0 = \delta S &= \delta \int_a^b \ell(\hat{\mathbf{v}}, \zeta, D, \rho) dt \\ &= \delta \int_a^b \int_{\mathcal{D}} \left(\frac{1}{2} \left(|\hat{\mathbf{v}}|^2 + \sigma^2 (\partial_t \zeta + \nabla_{\mathbf{r}} \zeta \cdot \hat{\mathbf{v}})^2 \right) - \frac{\rho_{ref}}{\rho} \frac{\zeta^2}{2Fr^2} \right) D\rho - p(D-1) d^2r dt. \end{aligned} \quad (2.5)$$

¹In [6] the potential energy was linear in ζ . This linearity neglected the restoring force due to vertical pressure gradient via Archimedes' principle. Adopting the potential energy quadratic in ζ regains this restoring force.

The advected quantities $D(\mathbf{r}, t)d^2r$ and $\rho(\mathbf{r}, t)$ evolve via push-forward by the horizontal flow map, ϕ_t . For example, $D_t d^2r_t = \phi_{t*}(D_0 d^2r_0)$ and $\rho_t = \phi_{t*}\rho_{ref}$ denote, respectively, evolution of the determinant of the Lagrange to Euler map and of the local scalar value of the mass density. Conservation of mass is then expressed as the push-forward relation, $D_t \rho_t d^2r_t = \phi_{t*}(D_0 \rho_{ref} d^2r_0)$. The pressure p in (2.5) acts as a Lagrange multiplier to enforce conservation of area, so that $D_t = 1 = \phi_{t*}D_0$, and the horizontal flow is incompressible, which implies that the horizontal velocity is divergence-free, i.e., $\operatorname{div}_{\mathbf{r}} \hat{\mathbf{v}}(\mathbf{r}, t) = 0$. Taking variations of the action integral (2.5) yields the following set of equations,

$$\begin{aligned} \delta \hat{\mathbf{v}} : \quad & \frac{\delta \ell}{\delta \hat{\mathbf{v}}} = D\rho(\hat{\mathbf{v}} \cdot d\mathbf{r} + \sigma^2 \hat{w} d\zeta) \otimes d^2r := D\rho \mathbf{V} \cdot d\mathbf{r} \otimes d^2r, \\ & \text{with } \hat{w} = \partial_t \zeta + \hat{\mathbf{v}} \cdot \nabla_{\mathbf{r}} \zeta, \\ \delta \zeta : \quad & \partial_t(\sigma^2 D\rho \hat{w}) + \operatorname{div}_{\mathbf{r}}(\sigma^2 D\rho \hat{w} \hat{\mathbf{v}}) - D \frac{\zeta \rho_{ref}}{Fr^2} = 0, \\ \delta D : \quad & \frac{\delta \ell}{\delta D} = \frac{\rho}{2}(|\hat{\mathbf{v}}|^2 + \sigma^2 \hat{w}^2) - \frac{\rho_{ref} \zeta^2}{2Fr^2} - p =: \rho \tilde{\omega} - \tilde{p}, \\ \delta \rho : \quad & \frac{\delta \ell}{\delta \rho} = \frac{D}{2}(|\hat{\mathbf{v}}|^2 + \sigma^2 \hat{w}^2) =: D \tilde{\omega}, \quad \tilde{p} := p + \frac{\rho_{ref} \zeta^2}{2Fr^2}, \\ \delta p : \quad & D - 1 = 0 \implies \operatorname{div}_{\mathbf{r}} \hat{\mathbf{v}} = 0. \end{aligned} \tag{2.6}$$

From their definitions as advected quantities, one also knows that D and ρ satisfy

$$\begin{aligned} (\partial_t + \mathcal{L}_{\hat{\mathbf{v}}})(D d^2r) = 0 & \implies \partial_t D + \operatorname{div}_{\mathbf{r}}(D \hat{\mathbf{v}}) = 0 \quad \text{with } D = 1, \\ (\partial_t + \mathcal{L}_{\hat{\mathbf{v}}})\rho = 0 & \implies \partial_t \rho + \hat{\mathbf{v}} \cdot \nabla_{\mathbf{r}} \rho = 0, \end{aligned} \tag{2.7}$$

where $\mathcal{L}_{\hat{\mathbf{v}}}$ denotes the Lie derivative operation along the horizontal velocity vector field, $\hat{\mathbf{v}}$, which provides coordinate-free brevity in the notation.

Theorem 1 (Kelvin-Noether circulation theorem). *Use of the Euler-Poincaré (EP) theorem yields the following Kelvin circulation theorem*

$$\frac{d}{dt} \oint_{c(\hat{\mathbf{v}})} (\hat{\mathbf{v}} \cdot d\mathbf{r} + \sigma^2 \hat{w} d\zeta) = - \oint_{c(\hat{\mathbf{v}})} \frac{1}{\rho} d\tilde{p}. \tag{2.8}$$

Proof. The Euler-Poincaré (EP) theorem in this case yields

$$(\partial_t + \mathcal{L}_{\hat{\mathbf{v}}}) \frac{\delta \ell}{\delta \hat{\mathbf{v}}} = \frac{\delta \ell}{\delta D} \diamond D + \frac{\delta \ell}{\delta \rho} \diamond \rho := D \nabla_{\mathbf{r}} \frac{\delta \ell}{\delta D} - \frac{\delta \ell}{\delta \rho} \nabla_{\mathbf{r}} \rho \tag{2.9}$$

Here the diamond (\diamond) operator is defined by

$$\left\langle \frac{\delta \ell}{\delta a} \diamond a, X \right\rangle_{\mathfrak{X}} =: \left\langle \frac{\delta \ell}{\delta a}, -\mathcal{L}_X a \right\rangle_V. \tag{2.10}$$

In addition, $X \in \mathfrak{X}$ is a (smooth) vector field defined on \mathbb{R}^2 and $a \in V$, a vector space of advected quantities, which are here the scalar function, ρ , and the areal density $D d^2r$. Using the advection relations for D and ρ in (2.7) and the corresponding variational derivatives in (2.6) simplifies the EP equation in (2.10) to

$$(\partial_t + \mathcal{L}_{\hat{\mathbf{v}}}) \left(\frac{1}{D\rho} \frac{\delta \ell}{\delta \hat{\mathbf{v}}} \right) = \frac{1}{\rho} \nabla_{\mathbf{r}} \frac{\delta \ell}{\delta D} - \frac{1}{D\rho} \frac{\delta \ell}{\delta \rho} \nabla_{\mathbf{r}} \rho. \tag{2.11}$$

Equation (2.6) then yields $(\partial_t + \mathcal{L}_{\hat{\mathbf{v}}})(\hat{\mathbf{v}} \cdot d\mathbf{r} + \sigma^2 \hat{w} d\zeta) = -\rho^{-1} d\tilde{p} + d\tilde{\omega}$.

Inserting the last relation into the following standard relation for the time derivative of a loop integral then completes the proof of equation (2.8) appearing in the statement of the theorem,

$$\frac{d}{dt} \oint_{c(\hat{\mathbf{v}})} (\hat{\mathbf{v}} \cdot d\mathbf{r} + \sigma^2 \hat{w} d\zeta) = \oint_{c(\hat{\mathbf{v}})} (\partial_t + \mathcal{L}_{\hat{\mathbf{v}}})(\hat{\mathbf{v}} \cdot d\mathbf{r} + \sigma^2 \hat{w} d\zeta) = \oint_{c(\hat{\mathbf{v}})} -\rho^{-1} d\tilde{p} + d\tilde{\omega}. \tag{2.12}$$

Using the advection relations for D and ρ in (2.7) again and combining with the variational relations with respect to ζ in (2.6) simplifies the \hat{w} and ζ equations, as follows.

$$\begin{aligned} (\partial_t + \mathcal{L}_{\hat{\mathbf{v}}})\hat{w} &= (\partial_t + \hat{\mathbf{v}} \cdot \nabla_{\mathbf{r}})\hat{w} = -\frac{\rho_{ref}}{\sigma^2 Fr^2 \rho} \zeta, \\ (\partial_t + \mathcal{L}_{\hat{\mathbf{v}}})\zeta &= (\partial_t + \hat{\mathbf{v}} \cdot \nabla_{\mathbf{r}})\zeta = \hat{w}. \end{aligned} \quad (2.13)$$

After deriving these equations, one may finally evaluate the constraint $D = 1$ imposed by the variation in pressure p to obtain further simplifications. \square

Corollary 2 (Kelvin-Noether circulation theorem for the current). *The Kelvin circulation theorem for the current alone is given by,*

$$\frac{d}{dt} \oint_{c(\hat{\mathbf{v}})} \hat{\mathbf{v}} \cdot d\mathbf{r} = - \oint_{c(\hat{\mathbf{v}})} \frac{1}{\rho} dp - d \frac{|\hat{\mathbf{v}}|^2}{2}. \quad (2.14)$$

Proof. Equation (2.14) follows by shifting the $\hat{w}d\zeta$ term in equation (2.34) to the right-hand side, as

$$\begin{aligned} \frac{d}{dt} \oint_{c(\hat{\mathbf{v}})} \hat{\mathbf{v}} \cdot d\mathbf{r} &= - \oint_{c(\hat{\mathbf{v}})} \frac{1}{\rho} d\tilde{p} + \sigma^2 (\partial_t + \mathcal{L}_{\hat{\mathbf{v}}})(\hat{w} d\zeta) - d\tilde{\omega} \\ &= - \oint_{c(\hat{\mathbf{v}})} \frac{1}{\rho} d\tilde{p} + \sigma^2 ((\partial_t + \hat{\mathbf{v}} \cdot \nabla_{\mathbf{r}})\hat{w})d\zeta + \sigma^2 \hat{w}d\hat{w} - d\tilde{\omega} \\ &= - \oint_{c(\hat{\mathbf{v}})} \frac{1}{\rho} d\tilde{p} - \frac{\rho_{ref}}{Fr^2 \rho} \zeta d\zeta + \sigma^2 \hat{w}d\hat{w} - d\tilde{\omega} \\ &= - \oint_{c(\hat{\mathbf{v}})} \frac{1}{\rho} dp - d \frac{|\hat{\mathbf{v}}|^2}{2} \\ &=: - \oint_{c(\hat{\mathbf{v}})} \frac{1}{\rho} dp - d \frac{|\hat{\mathbf{v}}|^2}{2}. \end{aligned} \quad (2.15)$$

\square

Remark 2.1 (Separation of wave and current circulation.). The decoupling of the Kelvin-Noether circulation theorem into its wave and current components, leading to the reduction of the current flow to the Euler result in equation (2.14), was also observed in [6]. This behaviour is consistent with the Carney-Drazin ‘non-acceleration’ theorem [4, 20]. Namely, in certain circumstances, wave activity does not create circulation in the mean current. A modification that allows exchange of circulation between wave (vertical) and current (horizontal) components of the flow was proposed in [6]. The instabilities observed around the edges of eddies in the satellite imagery shown in figure 1 suggests that a coupling of this sort may exist at high wave number.

Remark 2.2. It is clear from equations (2.34) – (2.14) that generation of circulation of the current by the dynamics in equation (2.11) requires non-zero $\nabla_{\mathbf{r}}\rho \times \nabla_{\mathbf{r}}p$. No current circulation is generated by wave variables in the case of constant buoyancy.

2.2 Thermal potential vorticity (TPV) dynamics on a free surface

The momentum map arising from the variations in (2.6) is given by

$$\frac{1}{D} \frac{\delta \ell}{\delta \hat{\mathbf{v}}} = \rho \hat{\mathbf{v}} \cdot d\mathbf{r} + \sigma^2 \rho \hat{w} d\zeta. \quad (2.16)$$

As expected from the well-known non-acceleration theorem [4, 20], the dynamics of the Euler-Poincaré equations separate (2.11) gives the dynamics of the fluid and wave components of the momentum one-form (2.16).

$$\begin{aligned} (\partial_t + \mathcal{L}_{\hat{v}}) \left(\rho (\hat{v} \cdot d\mathbf{r}) \right) &= -dp + \frac{\rho}{2} d(|\hat{v}|^2) \\ (\partial_t + \mathcal{L}_{\hat{v}}) (\sigma^2 \rho \hat{w} d\zeta) &= -\frac{\rho_{ref}}{Fr^2} \zeta d\zeta + \sigma^2 \rho \hat{w} d\hat{w}. \end{aligned} \quad (2.17)$$

The mass-weighted thermal potential vorticity (TPV) also separates into fluid and wave components $Q = Q_F + Q_W$ with following definitions

$$\begin{aligned} Q d^2r &= d \left(\rho (\hat{v} \cdot d\mathbf{r} + \sigma^2 \hat{w} d\zeta) \right) \\ &= d\rho \wedge (\hat{v} \cdot d\mathbf{r} + \sigma^2 \hat{w} d\zeta) + \rho \left(\hat{z} \cdot \operatorname{curl} \hat{v} + \sigma^2 J(\hat{w}, \zeta) \right) d^2r \\ &= \left(\operatorname{div}(\rho \nabla \psi) + \sigma^2 J(\rho \hat{w}, \zeta) \right) d^2r \quad \text{when } \hat{v} = \nabla^\perp \psi \quad \text{for } D = 1, \\ \text{with } Q_F &:= \operatorname{div}(\rho \nabla \psi), \quad Q_W = J(\sigma^2 \tilde{w}, \zeta). \end{aligned} \quad (2.18)$$

where buoyancy weighted vertical velocity is defined as $\tilde{w} := \rho \hat{w}$. The dynamics of $Q_F d^2r$ and $Q_W d^2r$ can be computed from (2.17) as

$$\begin{aligned} (\partial_t + \mathcal{L}_{\hat{v}})(Q_F d^2r) &= \frac{1}{2} d\rho \wedge d|\hat{v}|^2 = \frac{1}{2} J(\rho, |\nabla \psi|^2) d^2r, \\ (\partial_t + \mathcal{L}_{\hat{v}})(Q_W d^2r) &= \sigma^2 \frac{1}{2} d\rho \wedge d \left(\frac{\tilde{w}^2}{\rho^2} \right) = J \left(\rho, \frac{\sigma^2 \tilde{w}^2}{2\rho^2} \right) d^2r. \end{aligned} \quad (2.19)$$

The operator $\operatorname{div}(\rho \nabla)$ is invertible, so long as ρ is a differentiable positive function, which can be ensured by requiring that this condition holds initially. Consequently, the stream function ψ is related to the other fluid variables by

$$\psi := (\operatorname{div} \rho \nabla)^{-1} Q_F. \quad (2.20)$$

The potential vorticity dynamics can then be written in coordinate form as

$$\begin{aligned} \partial_t Q_F + J(\psi, Q_F) &= J \left(\rho, \frac{1}{2} |\nabla \psi|^2 \right), \\ \partial_t Q_W + J(\psi, Q_W) &= J \left(\rho, \frac{\sigma^2 \tilde{w}^2}{2\rho^2} \right), \\ \text{with } Q_F &:= \operatorname{div}(\rho \nabla \psi) \quad \text{and } Q_W := J(\sigma^2 \tilde{w}, \zeta), \\ \partial_t \rho + J(\psi, \rho) &= 0, \\ \partial_t \zeta + J(\psi, \zeta) &= \hat{w} =: \tilde{w}/\rho, \\ \partial_t (\sigma^2 \tilde{w}) + J(\psi, \sigma^2 \tilde{w}) &= -\frac{\rho_{ref} \zeta}{Fr^2}. \end{aligned} \quad (2.21)$$

Theorem 3. *The Legendre transform yields the Hamiltonian formulation of our system of wave-current equations (2.21), which with $\tilde{w} = \rho \hat{w}$ may be written in the untangled block-diagonal Poisson form as*

$$\frac{\partial}{\partial t} \begin{bmatrix} Q \\ \rho \\ \sigma^2 \tilde{w} \\ \zeta \end{bmatrix} = \begin{bmatrix} J(Q, \cdot) & J(\rho, \cdot) & 0 & 0 \\ J(\rho, \cdot) & 0 & 0 & 0 \\ 0 & 0 & 0 & -1 \\ 0 & 0 & 1 & 0 \end{bmatrix} \begin{bmatrix} \delta h / \delta Q = \psi \\ \delta h / \delta \rho = \tilde{w} \\ \delta h / \delta (\sigma^2 \tilde{w}) = \tilde{w} / \rho + J(\zeta, \psi) \\ \delta h / \delta \zeta = -J(\sigma^2 \tilde{w}, \psi) + \frac{\rho_{ref} \zeta}{Fr^2} \end{bmatrix}. \quad (2.22)$$

The energy Hamiltonian $h(Q, \rho, \hat{w}, \zeta)$ associated with this system is given by

$$\begin{aligned} h(Q, \rho, \tilde{w}, \zeta) &= \int \frac{1}{2} \left(Q - J(\sigma^2 \tilde{w}, \zeta) \right) (\operatorname{div} \rho \nabla)^{-1} \left(Q - J(\sigma^2 \tilde{w}, \zeta) \right) \\ &\quad + \left(\frac{\sigma^2 \tilde{w}^2}{2\rho^2} + \frac{\rho_{ref}}{\rho} \frac{\zeta^2}{2Fr^2} \right) \rho d^2r. \end{aligned} \quad (2.23)$$

Theorem 4 (Casimir functions). *The Casimir functions, conserved by the relation $\{C_{\Phi,\Psi}, h\} = 0$ with any Hamiltonian $h(\mathbf{M}, D)$ for the block-diagonal Lie-Poisson bracket in equation (2.22) are given by*

$$C_{\Phi,\Psi} := \int \Phi(\rho) + Q\Psi(\rho) d^2r \quad (2.24)$$

Proof. The Casimirs $C_{\Phi,\Psi}$ for the direct sum of the Lie-Poisson brackets for Q and ρ and canonical Poisson brackets for \tilde{w} and ζ follows by direct verification that the $C_{\Phi,\Psi}$ are conserved for any differentiable functions, (Φ, Ψ) . \square

2.3 WCIFS equations in the slowly varying envelope (SVE) approximation

The SVE solutions apply to satellite observations of sea surface waves. From the viewpoint of satellite observations, the vertical motion on the sea surface typically oscillates much more quickly than the rate of change of features in the horizontal motion of the ocean surface currents. In this situation, the standard WKB approximation introduces a solution Ansatz for the slowly varying envelope (SVE) of the rapidly oscillating vertical wave elevation in the form,

$$\zeta(\mathbf{r}, t) = \Re \left(a(\mathbf{r}, t) \exp \left(\frac{i\theta(\mathbf{r}, t)}{\epsilon} \right) \right) \quad \text{with } \epsilon \ll 1. \quad (2.25)$$

The SVE solution Ansatz (2.25) comprises the product of a slowly varying complex amplitude $a(\mathbf{r}, t) \in \mathbb{C}$ multiplied by a rapidly oscillating phase $\theta(\mathbf{r}, t)/\epsilon \in \mathbb{R}$ with $\epsilon \ll 1$ in which the phase factor $\theta(\mathbf{r}, t)$ may also vary slowly as a function of the space and time variables, (\mathbf{r}, t) .

Following [9], let us substitute the SVE solution Ansatz (2.25) into Hamilton's principle in (2.5) and find the condition on the parameter $\epsilon \ll 1$ that will allow higher order wave terms to be neglected. For this, one computes

$$\begin{aligned} 0 = \delta S_{SVE} &= \delta \int_a^b \ell_{SVE}(\hat{\mathbf{v}}, D, \rho; a, \theta) dt \\ &= \delta \int_a^b \int_{\mathcal{D}} \frac{1}{2} D\rho |\hat{\mathbf{v}}|^2 - p(D-1) + \frac{\sigma^2}{2} D\rho \left(\left(\frac{d\zeta}{dt} \right)^2 - \frac{\rho_{ref}}{\rho} \frac{\zeta^2}{2\sigma^2 Fr^2} \right) d^2r dt \\ &= \delta \int_a^b \int_{\mathcal{D}} \frac{1}{2} D\rho |\hat{\mathbf{v}}|^2 - p(D-1) \\ &\quad + \frac{\sigma^2}{8} D\rho \left(\left| \frac{da}{dt} \right|^2 + \frac{2}{\epsilon} \frac{d\theta}{dt} \Im \left(a^* \frac{da}{dt} \right) + \frac{|a|^2}{\epsilon^2} \left(\left(\frac{d\theta}{dt} \right)^2 - \frac{\rho_{ref}}{\rho} \frac{\epsilon^2}{\sigma^2 Fr^2} \right) \right) d^2r dt \\ &\approx \delta \int_a^b \int_{\mathcal{D}} \frac{1}{2} D\rho |\hat{\mathbf{v}}|^2 - p(D-1) \\ &\quad + \frac{\sigma^2 |a|^2}{8\epsilon^2} D\rho \left((\partial_t \theta + \hat{\mathbf{v}} \cdot \nabla_{\mathbf{r}} \theta)^2 - \frac{\rho_{ref}}{\rho} \frac{\epsilon^2}{\sigma^2 Fr^2} \right) d^2r dt + O\left(\frac{\sigma^2}{\epsilon}\right). \end{aligned} \quad (2.26)$$

The leading order wave term in Hamilton's principle will dominate the solution and the remaining wave terms may be neglected, when ²

$$\epsilon \ll 1, \quad \frac{\epsilon^2}{\sigma^2 Fr^2} \approx 1, \quad \text{and} \quad \sigma^2 Fr^2 \ll 1. \quad (2.27)$$

According to the estimates in (2.3) there is a range of physical parameters relevant to satellite observations in which the SVE approximation applies, for $\sigma^2 Fr^2 \ll 1$.

²The ratio $\frac{\epsilon^2}{\sigma^2 Fr^2} \approx 1$ is required for the time scales of the currents and the waves to match.

To continue the investigation of the SVE description of wave-current interactions on the sea surface, we take variations of the action integral (2.27) to find the following set of equations,

$$\begin{aligned}
\delta\hat{\mathbf{v}} : \quad & \frac{\delta\ell}{\delta\hat{\mathbf{v}}} = D\rho\left(\hat{\mathbf{v}} \cdot d\mathbf{r} + \mathcal{N}d\frac{d\theta}{dt}\right) \otimes d^2r \quad \text{with} \quad \mathcal{N} := \frac{\sigma^2|a|^2}{4\epsilon^2}, \\
\delta|a|^2 : \quad & \frac{\delta\ell}{\delta|a|^2} = \frac{\sigma^2}{8Fr^2}D\rho\left(\left(\frac{d\theta}{dt}\right)^2 - \frac{\rho_{ref}}{\rho}\right) = 0 \quad \text{at} \quad O\left(\frac{\sigma^2}{\epsilon^2}\right) \\
& \implies \frac{d\theta}{dt} =: -\omega + \hat{\mathbf{v}} \cdot \mathbf{k} = \pm \frac{\sqrt{\rho\rho_{ref}}}{\rho} \quad \text{with} \quad \omega(\mathbf{r}, t) = -\partial_t\theta \quad \text{and} \quad \mathbf{k}(\mathbf{r}, t) = \nabla_{\mathbf{r}}\theta, \\
\delta\theta : \quad & \frac{\delta\ell}{\delta\theta} = 0 \implies \partial_t\mathcal{A} + \text{div}(\mathcal{A}\hat{\mathbf{v}}) = 0, \quad \text{with} \quad \mathcal{A} := D\rho\mathcal{N}\frac{d\theta}{dt} \quad \text{and} \quad \mathcal{N} := \frac{\sigma^2|a|^2}{4\epsilon^2}, \\
\delta D : \quad & \frac{\delta\ell}{\delta D} = \frac{\rho}{2}|\hat{\mathbf{v}}|^2 - p, \\
\delta\rho : \quad & \frac{\delta\ell}{\delta\rho} = \frac{D}{2}|\hat{\mathbf{v}}|^2, \\
\delta p : \quad & D - 1 = 0 \implies \text{div}_{\mathbf{r}}\hat{\mathbf{v}} = 0, \quad \text{Hence,} \quad \partial_t\mathcal{A} + \hat{\mathbf{v}} \cdot \nabla_{\mathbf{r}}\mathcal{A} = 0 \implies \partial_t|a|^2 + \hat{\mathbf{v}} \cdot \nabla_{\mathbf{r}}|a|^2 = 0.
\end{aligned} \tag{2.28}$$

In the second line of (2.28) we see that stationarity of the action integral with respect to variations in $|a|^2$ acts as a Lagrange multiplier to impose a constraint which relates the dynamics of the wave phase θ to the buoyancy. This constraint relation involves the Doppler-shifted frequency of the waves, as shown in the third line of (2.28). In combination with conservation of the wave action density and the divergence free condition on the fluid flow velocity $\hat{\mathbf{v}}$, this constraint relation implies in the last line of (2.28) that the wave magnitude $|a|^2$ is advected by the fluid flow. Because of the oscillatory nature of the solution Ansatz (2.25), the sign of the wave phase in $d\theta/dt = \partial_t\theta + \hat{\mathbf{v}} \cdot \nabla_{\mathbf{r}}\theta$ in the second line above is immaterial. Hence, hereafter, we will choose the positive root for $d\theta/dt = \sqrt{\rho\rho_{ref}}/\rho$.

From the conservation of wave action density \mathcal{A} in (2.28) and the definitions of the advected fluid variables, one finds that $|a|^2$, D and ρ satisfy the following advection relations

$$\begin{aligned}
(\partial_t + \mathcal{L}_{\hat{\mathbf{v}}})(Dd^2r) &= 0 \implies \partial_tD + \text{div}_{\mathbf{r}}(D\hat{\mathbf{v}}) = 0 \quad \text{with} \quad D = 1, \\
(\partial_t + \mathcal{L}_{\hat{\mathbf{v}}})\rho &= 0 \implies \partial_t\rho + \hat{\mathbf{v}} \cdot \nabla_{\mathbf{r}}\rho = 0, \\
(\partial_t + \mathcal{L}_{\hat{\mathbf{v}}})|a|^2 &= 0 \implies \partial_t|a|^2 + \hat{\mathbf{v}} \cdot \nabla_{\mathbf{r}}|a|^2 = 0,
\end{aligned} \tag{2.29}$$

where $\mathcal{L}_{\hat{\mathbf{v}}}$ denotes the Lie derivative operation along the horizontal velocity vector field, $\hat{\mathbf{v}}$. The Lie derivative notation $\mathcal{L}_{\hat{\mathbf{v}}}$ provides coordinate-free brevity in proving the following Kelvin circulation theorem for thermal wave-current theory.

Theorem 5 (Kelvin-Noether circulation theorem). *The variational equations in (2.28) imply the following Kelvin circulation theorem*

$$\frac{d}{dt} \oint_{c(\hat{\mathbf{v}})} \left(\hat{\mathbf{v}} \cdot d\mathbf{r} + \mathcal{N}d\frac{d\theta}{dt} \right) = - \oint_{c(\hat{\mathbf{v}})} \frac{1}{\rho} dp. \tag{2.30}$$

Proof. The Euler-Poincaré (EP) theorem [14] in this case yields

$$(\partial_t + \mathcal{L}_{\hat{\mathbf{v}}})\frac{\delta\ell}{\delta\hat{\mathbf{v}}} = \frac{\delta\ell}{\delta D} \diamond D + \frac{\delta\ell}{\delta\rho} \diamond \rho := D\nabla_{\mathbf{r}}\frac{\delta\ell}{\delta D} - \frac{\delta\ell}{\delta\rho}\nabla_{\mathbf{r}}\rho. \tag{2.31}$$

Here, the diamond (\diamond) operator is defined for a fluid advected quantity f by

$$\left\langle \frac{\delta\ell}{\delta f} \diamond f, X \right\rangle_{\mathfrak{X}} =: \left\langle \frac{\delta\ell}{\delta f}, -\mathcal{L}_X f \right\rangle_V. \tag{2.32}$$

In (2.32), $X \in \mathfrak{X}(\mathbb{R}^2)$ is a (smooth) vector field defined on \mathbb{R}^2 and $f \in V$ is a vector space of advected quantities. These advected quantities are the scalar function, ρ , and the areal density, Dd^2r .

Upon using the advection relations for D and ρ in (2.29) and the corresponding variational derivatives in (2.28), the EP equation in (2.31) simplifies to

$$(\partial_t + \mathcal{L}_{\hat{\mathbf{v}}})\left(\frac{1}{D\rho} \frac{\delta\ell}{\delta\hat{\mathbf{v}}}\right) = \frac{1}{\rho} \nabla_{\mathbf{r}} \frac{\delta\ell}{\delta D} - \frac{1}{D\rho} \frac{\delta\ell}{\delta\rho} \nabla_{\mathbf{r}} \rho. \quad (2.33)$$

$$\text{Equation (2.28) then yields } (\partial_t + \mathcal{L}_{\hat{\mathbf{v}}})\left(\hat{\mathbf{v}} \cdot d\mathbf{r} + \mathcal{N}d\frac{d\theta}{dt}\right) = -\rho^{-1}dp + d\left(\frac{1}{2}|\hat{\mathbf{v}}|^2\right).$$

Inserting the last relation into the following standard relation for the time derivative of a loop integral then completes the proof of equation (2.30) appearing in the statement of the theorem,

$$\frac{d}{dt} \oint_{c(\hat{\mathbf{v}})} \left(\hat{\mathbf{v}} \cdot d\mathbf{r} + \mathcal{N}d\frac{d\theta}{dt}\right) = \oint_{c(\hat{\mathbf{v}})} (\partial_t + \mathcal{L}_{\hat{\mathbf{v}}})\left(\hat{\mathbf{v}} \cdot d\mathbf{r} + \mathcal{N}d\frac{d\theta}{dt}\right) = \oint_{c(\hat{\mathbf{v}})} -\rho^{-1}dp + d\left(\frac{1}{2}|\hat{\mathbf{v}}|^2\right). \quad (2.34)$$

Note, however, that equations (2.28) imply the following combination of advected quantities,

$$(\partial_t + \mathcal{L}_{\hat{\mathbf{v}}})\left(\mathcal{N}d\frac{d\theta}{dt}\right) = \frac{\sigma^2}{4Fr^2}(\partial_t + \mathcal{L}_{\hat{\mathbf{v}}})\left(|a|^2d\sqrt{\frac{\rho_{ref}}{\rho}}\right) = 0. \quad (2.35)$$

Consequently, the wave-momentum 1-form $\mathcal{N}d(\frac{d\theta}{dt})$ is advected by the fluid flow and the Kelvin circulation theorem in equation (2.34) reduces to the standard circulation theorem for the 2D Euler fluid equations. \square

Remark 2.3 (Separation of wave and current motion in the SVE approximation). The decoupling of the Kelvin-Noether circulation theorem into its wave and current components for the SVE approximation is inherited from the un-approximated model. When modifications to the un-approximated model which removes this property are added, one would expect the new SVE approximation to lose the non-acceleration result.

Remark 2.4. Equation (2.35) implies advection of the 1-form $|a|^2d\rho$, which in turn implies advection of the Jacobian $J(|a|^2, \rho)$. Since the fluid flow is area preserving, $\text{div}\hat{\mathbf{v}} = 0$, the following 2-form will also be advected,

$$(\partial_t + \hat{\mathbf{v}} \cdot \nabla_{\mathbf{r}})\left(d|a|^2 \wedge d\rho\right) = 0. \quad (2.36)$$

Thus, the divergence-free flow of $\hat{\mathbf{v}}$ preserves the area element $d|a|^2 \wedge d\rho$. This means that if the gradients $\nabla|a|^2$ and $\nabla\rho$ are not aligned initially, then they will remain so. It also means that equilibrium solutions of (2.36) will be symplectic manifolds [12].

After deriving these equations, one may finally evaluate the constraint $D = 1$ imposed by the variation in pressure p to obtain further simplifications.

2.4 Thermal potential vorticity dynamics with SVE on a free surface

The momentum map arising from the variations of the action in (2.28) is given by

$$\begin{aligned} \frac{1}{D} \frac{\delta\ell}{\delta\hat{\mathbf{v}}} &= \rho\left(\hat{\mathbf{v}} \cdot d\mathbf{r} + \mathcal{N}d\frac{d\theta}{dt}\right) \quad \text{with} \quad \mathcal{N} := \frac{\sigma^2 N^2 |a|^2}{4} =: \Gamma |a|^2 \quad \text{and} \quad \frac{d\theta}{dt} = \sqrt{\frac{\rho_{ref}}{\rho}} \\ \text{so} \quad \frac{1}{D} \frac{\delta\ell}{\delta\hat{\mathbf{v}}} &= \rho\left(\hat{\mathbf{v}} \cdot d\mathbf{r} + \Gamma |a|^2 d(\sqrt{\rho\rho_{ref}}/\rho)\right) \end{aligned} \quad (2.37)$$

According to the Euler-Poincaré equation (2.33), the dynamics of the fluid and wave components of the 1-form in (2.37) *separates* into the following equations,

$$\begin{aligned} (\partial_t + \mathcal{L}_{\hat{\mathbf{v}}})\left(\rho(\hat{\mathbf{v}} \cdot d\mathbf{r})\right) &= -dp + \frac{\rho}{2}d(|\hat{\mathbf{v}}|^2) \\ (\partial_t + \mathcal{L}_{\hat{\mathbf{v}}})\left(|a|^2 d\sqrt{\rho\rho_{ref}}\right) &= 0. \end{aligned} \quad (2.38)$$

This means that the mass-weighted thermal potential vorticity (TPV) dynamics also separates into the following fluid and wave components, $Q = Q_F + Q_W$, given by

$$\begin{aligned} Q d^2r &:= d\left(\rho\left(\hat{\mathbf{v}} \cdot d\mathbf{r} + \Gamma|a|^2 d\sqrt{\frac{\rho_{ref}}{\rho}}\right)\right) \\ &= \left(\operatorname{div}(\rho\nabla\psi) - \Gamma J\left(|a|^2, \sqrt{\rho\rho_{ref}}\right) d^2r\right) \quad \text{when } \hat{\mathbf{v}} = \nabla^\perp\psi \quad \text{for } D = 1, \\ &= Q_F d^2r + Q_W d^2r, \end{aligned} \quad (2.39)$$

with $Q_F := \operatorname{div}(\rho\nabla\psi)$ and $Q_W := \Gamma J\left(\sqrt{\rho\rho_{ref}}, |a|^2\right)$.

Then, again, the differentials of the separate equations in (2.38) yield the ‘non-acceleration’ result,

$$\begin{aligned} (\partial_t + \mathcal{L}_{\hat{\mathbf{v}}})(Q_F d^2r) &= \frac{1}{2} d\rho \wedge d|\hat{\mathbf{v}}|^2 = \frac{1}{2} J(\rho, |\nabla\psi|^2) d^2r, \\ (\partial_t + \mathcal{L}_{\hat{\mathbf{v}}})(Q_W d^2r) &= 0 \end{aligned} \quad (2.40)$$

Equivalently, in coordinates one has

$$\begin{aligned} \partial_t Q_F + \hat{\mathbf{v}} \cdot \nabla Q_F &= \frac{1}{2} J(\rho, |\nabla\psi|^2), \\ \partial_t Q_W + \hat{\mathbf{v}} \cdot \nabla Q_W &= 0, \\ \text{with } Q_F &:= \operatorname{div}(\rho\nabla\psi) \quad \text{and} \quad Q_W := \Gamma J\left(\sqrt{\rho\rho_{ref}}, |a|^2\right), \\ \partial_t \rho + \hat{\mathbf{v}} \cdot \nabla_{\mathbf{r}} \rho &= 0 \quad \text{and} \quad \Gamma = \frac{\sigma^2}{4Fr^2} = O(1), \\ \partial_t |a|^2 + \hat{\mathbf{v}} \cdot \nabla_{\mathbf{r}} |a|^2 &= 0, \\ \partial_t \theta + \hat{\mathbf{v}} \cdot \nabla_{\mathbf{r}} \theta &= \frac{\sqrt{\rho\rho_{ref}}}{\rho}. \end{aligned} \quad (2.41)$$

The operator $(\operatorname{div}\rho\nabla)$ is invertible, so long as ρ is a differentiable positive function, which can be ensured by requiring that this condition holds initially, since ρ is advected. Consequently, the stream function ψ is related to the other fluid variables by

$$\psi := (\operatorname{div}\rho\nabla)^{-1} Q_F. \quad (2.42)$$

The dynamics of the equation set (2.41) explains why the various physical components of the flow coordinate their movements, as seen in satellite observations in figure 2. In particular, the motion of buoyancy ρ and squared wave amplitude $|a|^2$ are coordinated with each other through the advection of the momentum 1-form $|a|^2 d\rho$ and the area 2-form $d|a|^2 \wedge d\rho$. Likewise the the motion of the fluid potential vorticity Q_F and the mass density ρ are coordinated with each other through the mass-weighted definition of the stream function in (2.42). These considerations emphasise again the importance of horizontal buoyancy gradients in sea surface dynamics.

3 Numerical implementation

Our implementation of the WCIFS equations (2.21) and the WCIFS equations in the SVE approximation (2.41) used the finite element method (FEM) for the spatial variables. The FEM algorithm we used is based on the algorithm formulated in [13] and is implemented using the Firedrake ³ software. In particular, for (2.21) we approximated the fluid potential vorticity Q_F , buoyancy ρ , wave elevation ζ and buoyancy weighted wave vertical velocity \tilde{w} using a first order discrete Galerkin finite element space. Similarly, for (2.41), we approximated Q_F , ρ , square of the wave amplitude $|a|^2$ and wave phase θ using a first order discrete Galerkin finite element space. The stream function ψ for both models was approximated by using a first order continuous Galerkin finite element space. For the time integration, we used the third order strong stability preserving Runge Kutta method [10].

³<https://firedrakeproject.org/index.html>

Figures 3 and 4 present snapshots of high resolution runs of the WCIFS equations and the WCIFS equations in the SVE approximation. These simulations were run with the following parameters. The domain is $[0, 1]^2$ at a resolution of 512^2 . The boundary conditions are periodic in the x direction, and homogeneous Dirichlet for ψ in the y direction. To see the effects of the waves on the currents, the procedure was divided into two stages for both set of equations. The first stage was performed without wave activity for $T_{spin} = 100$ time units starting from the following initial conditions

$$\begin{aligned} Q_F(x, y, 0) &= \sin(8\pi x) \sin(8\pi y) + 0.4 \cos(6\pi x) \cos(6\pi y) + 0.3 \cos(10\pi x) \cos(4\pi y) + \\ &\quad 0.02 \sin(2\pi y) + 0.02 \sin(2\pi x), \\ \rho(x, y, 0) &= 1 + 0.2 \sin(2\pi x) \sin(2\pi y) \quad \text{and} \quad \rho_{ref} = 1. \end{aligned} \quad (3.1)$$

The purpose of the first stage was to allow the system to spin up to a statistically steady state without any wave activity. The PV and buoyancy variables at the end of the initial spin-up period are denoted as $Q_{spin}(x, y) = Q_F(x, y, T_{spin})$ and $\rho_{spin}(x, y) = \rho(x, y, T_{spin})$. Figures of these variables are shown in figure 5. In the second stage, the full simulations including the wave variables were run with the

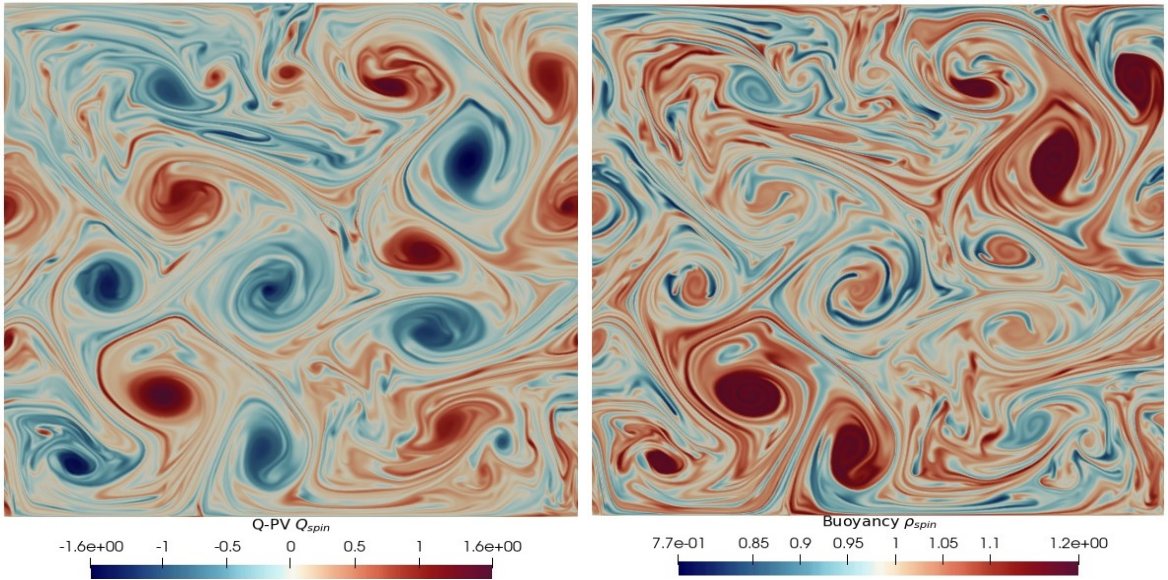


Figure 5: These figures show the results of the first stage of the simulation in which only fluid motion is present and the wave degrees of freedom are absent. The panels show fluid potential vorticity Q_F (left) and buoyancy ρ (right). The fluid state obtained from the first stage was used as the initial condition for the second stage simulations in which wave variables were included. These distributions of fluid properties show strong spatial coherence. The coordination of wave and fluid properties that emerges in the second stage of the simulations shown in Figure 3 and 4 arises from the interaction between the wave and current components of the flow which is mediated by the buoyancy gradient.

initial conditions for the flow variables being the state achieved at the end of the first stage. To start the second stage for (2.21), wave variables were introduced with the following initial conditions

$$\begin{aligned} \zeta(x, y, 0) &= \sin(8\pi x) \sin(8\pi y) + 0.4 \cos(6\pi x) \cos(6\pi y) + 0.3 \cos(10\pi x) \cos(4\pi y) + \\ &\quad 0.02 \sin(2\pi y) + 0.02 \sin(2\pi x), \\ \tilde{w}(x, y, 0) &= 0, \quad Q_F(x, y, 0) = Q_{spin}(x, y), \quad \rho(x, y, 0) = \rho_{spin}(x, y), \\ \sigma^2 Fr^2 &= 10^{-2}. \end{aligned} \quad (3.2)$$

To start the second stage for (2.41), wave variables were introduced with the following initial conditions

$$\begin{aligned} |a|^2(x, y, 0) &= (\sin(8\pi x) \sin(8\pi y) + 0.4 \cos(6\pi x) \cos(6\pi y) + 0.3 \cos(10\pi x) \cos(4\pi y) + \\ &\quad 0.02 \sin(2\pi y) + 0.02 \sin(2\pi x))^2, \\ \theta(x, y, 0) &= 0, \quad Q_F(x, y, 0) = Q_{spin}(x, y), \quad \rho(x, y, 0) = \rho_{spin}(x, y). \end{aligned} \quad (3.3)$$

Remark 3.1. Importantly, the wave phase θ in the second stage was set initially to zero. Thereafter, the wave phase θ increased linearly in time in proportion to the advected quantity $\sqrt{\rho\rho_{ref}}/\rho$ following each flow line, as implied by the last equation in (2.41).

4 Conclusion and Outlook

This paper models the effects of thermal fronts on the dynamics of the ocean's waves and currents. It introduces and simulates two models of thermal wave-current dynamics on a free surface. The original WCIFS model is derived from Hamilton's principle via the composition of two maps which represent the horizontal and vertical motion respectively. The second, a slowly varying envelope (SVE) model, is introduced via the standard WKB approximation which takes advantage of large separation of the space-time scales between the slow horizontal currents and fast vertical oscillations. In particular, the second model introduces the WKB solution Ansatz into Hamilton's principle, whereupon the time integral averages over the phases of the rapid oscillations that are out of resonance with the slowly varying envelope. Model runs of both models are presented in which the buoyancy mediates the dynamics of the currents and waves, as seen in Figures 3 and 4. These simulations also validate the use of the WKB approximation for two reasons. First, the resolved small scale wave features of the original WCIFS model lie primarily within the envelope defined by the SVE approximate model. This means that the dynamics of the spatial features of the SVE approximate model are consistent with those of the original WCIFS model, although the resolved space and time scales differ. Secondly, requiring that $\epsilon^2/(Fr^2\sigma^2) = O(1)$ ensures that the time scale for the wave envelope dynamics matches that for the fluid motion.

Nonetheless, the two models introduced here merit further study in several directions. For example, it remains to: (1) quantify the correlations observed visually; (2) determine their rate of formation; and (3) parameterise the model for comparison and analysis of the satellite data on which their derivations were based. Furthermore, the models discussed here involve only variables that are evaluated on the free surface and therefore they neglect bathymetry. A scientific challenge persists in understanding regions of the ocean where bathymetry has profound effects on the observable surface dynamics, such as in the Lofoten vortex [18]. This is a multiscale issue that might be addressed by including mesoscale modulations of the sub-mesoscale models derived here. One candidate for providing the mesoscale modulations would be the thermal quasi-geostrophic (TQG) model in which bathymetry has recently been included [13].

As mentioned in Remark 2.1, the wave component of the model presented here does not create circulation in the currents. The instabilities present in satellite simulations indicate that additional modelling is needed to fully capture this effect. Future work will investigate approaches for modelling these instabilities.

Many other questions remain about wave-current interaction. The full extent of submesoscale ocean dynamics is by no means adequately described by existing models. For example, we have little understanding of the formation and dynamics of various sea-surface phenomena, including the so-called 'spirals on the sea' [16]. Other questions are emerging because the ocean has absorbed in excess of 90% of the heat present in the earth system as a result of human activity during the post-industrial era [17]. The absorption of heat from the warming atmosphere is ongoing and it is forecast to become more dramatic. This absorption has resulted in 'marine heat waves', which are predicted to increase in frequency and severity. These changes to the upper ocean, where most of this heat is stored, could have a profound effect on the dynamical landscape of our oceans. These effects may, in turn, influence our weather and climate systems. Over the millennia, the ocean has approached statistical equilibrium under its current forcing conditions. Using modelling terminology, one says the ocean is well 'spun-up'. However, the continued warming of the ocean is likely to influence the number and intensity of thermal fronts. One hopes that mathematical models will provide a useful framework for estimating some of the potential impacts of these thermal fronts on atmospheric effects, as well.

Acknowledgements

We are grateful to our friends and colleagues who have generously offered their time, thoughts, and encouragement in the course of this work during the time of COVID-19. Thanks to A. Arnold, B. Chapron, D. Crisan, B. Fox-Kemper, E. Luesink, A. Mashayekhi, and J. C. McWilliams for their thoughtful comments and discussions. Particular thanks to B. Chapron, for providing the satellite data for several of the figures. The authors are grateful for partial support, as follows. DH for European Research Council (ERC) Synergy grant STUOD - DLV-856408; RH for the EPSRC scholarship (Grant No. EP/R513052/1); and OS for the EPSRC Centre for Doctoral Training in the Mathematics of Planet Earth (Grant No. EP/L016613/1).

References

- [1] Bühler., 2014. *Waves and mean flows*. Cambridge University Press.
- [2] Burby, J.W. and Ruiz, D.E., 2020. Variational nonlinear WKB in the Eulerian frame. *Journal of Mathematical Physics*, 61(5), p.053101.
- [3] Chapron, B., Kudryavtsev, V.N., Collard, F., Rasclle, N., Kubryakov, A.A. and Stanichny, S.V., 2020. Studies of Sub-Mesoscale Variability of the Ocean Upper Layer Based on Satellite Observations Data. *Physical Oceanography*, 27(6), pp.619-630. <https://archimer.ifremer.fr/doc/00682/79420/82002.pdf>
- [4] Charney, J. G. and P. G. Drazin, 1961: Propagation of planetary-scale disturbances from the lower into the upper atmosphere. *J. Geophys. Res.*, 66, 83-110.
- [5] Craig, W., 2016. On the Hamiltonian for water waves. arXiv preprint [arXiv:1612.08971](https://arxiv.org/abs/1612.08971).
- [6] Crisan, D., Holm, D.D. and Street, O.D., 2021. Wave-current interaction on a free surface. *Stud Appl Math.* 147:1277-1338. <https://doi.org/10.1111/sapm.12425>
- [7] Dong, J., Fox-Kemper, B., Zhang, H. and Dong, C., 2020. The scale of submesoscale baroclinic instability globally. *Journal of Physical Oceanography*, 50(9), pp.2649-2667. <https://doi.org/10.1175/JPO-D-20-0043.1>
- [8] Fox-Kemper, B., Johnson, L. and Qiao, F., 2022. Ocean near-surface layers. In *Ocean Mixing* (pp. 65-94). Elsevier.
- [9] Gjaja, I. and Holm, D.D., 1996. Self-consistent wave-mean flow interaction dynamics and its Hamiltonian formulation for a rotating stratified incompressible fluid, *Physica D*, **98** 343-378. [https://doi.org/10.1016/0167-2789\(96\)00104-2](https://doi.org/10.1016/0167-2789(96)00104-2)
- [10] Gottlieb, S. On High Order Strong Stability Preserving Runge–Kutta and Multi Step Time Discretizations. *J Sci Comput* 25, 105–128 (2005). <https://doi.org/10.1007/s10915-004-4635-5>
- [11] Gula, J., Taylor, J., Shcherbina, A. and Mahadevan, A., 2022. Submesoscale processes and mixing. In *Ocean Mixing* (pp. 181-214). Elsevier.
- [12] Holm, D.D., 2011. *Geometric mechanics-Part I: Dynamics and symmetry*. World Scientific Publishing Company.
- [13] Holm, D.D., Luesink, E and Pan, W, 2021. Stochastic mesoscale circulation dynamics in the thermal ocean. *Physics of Fluids*, 33, 046603. <https://doi.org/10.1063/5.0040026>
- [14] Holm, D.D., Marsden, J.E. and Ratiu, T.S., 1998. The Euler–Poincaré equations and semidirect products with applications to continuum theories. *Advances in Mathematics*, 137(1), pp.1-81. <https://doi.org/10.1006/aima.1998.1721>

[15] Morrow, R., Fu, L.-L., Ardhuin, F., Benkiran, M., Chapron, B., Cosme, E., d'Ovidio, F., Farrar, J.T., Gille, S.T. [et al.], 2019. Global Observations of Fine-Scale Ocean Surface Topography with the Surface Water and Ocean Topography (SWOT) Mission. *Frontiers in Marine Science*, 6, 232. <https://doi:10.3389/fmars.2019.00232>

[16] Munk, W., Armi, L., Fischer, K. and Zachariasen, F., 2000. Spirals on the sea. *Proceedings of the Royal Society of London. Series A: Mathematical, Physical and Engineering Sciences*, 456(1997), pp.1217-1280.

[17] H.-O. Pörtner, D.C. Roberts, V. Masson-Delmotte, P. Zhai, M. Tignor, E. Poloczanska, K. Mintenbeck, A. Alegría, M. Nicolai, A. Okem, J. Petzold, B. Rama, N.M. Weyer (eds.), 2019. *IPCC Special Report on the Ocean and Cryosphere in a Changing Climate*. In press.

[18] Volkov, D. L., Kubryakov, A. A., and Lumpkin, R., Formation and variability of the Lofoten basin vortex in a high-resolution ocean model, *Deep Sea Res., Part I* 105, 142–157 (2015). <https://doi.org/10.1016/j.dsr.2015.09.001>, Google Scholar

[19] Voronovich, A. G. (1976), Propagation of internal and surface gravity waves in the approximation of geometrical optics, *Izv. Atmos. Ocean. Phys.*, 12 p. 850-857.

[20] White, A.A., 1986. Finite amplitude, steady Rossby waves and mean flows: Analytical illustrations of the Charney-Drazin non-acceleration theorem. *Quarterly Journal of the Royal Meteorological Society*, 112(473), pp.749-773. <https://doi.org/10.1002/qj.49711247311>

[21] Whitham, G.B., 1967. Variational Methods and Applications to Water Waves, *Proc. Roy. Soc. London. Series A, Mathematical and Physical Sciences*, Vol. 299, No. 1456, A Discussion on Nonlinear Theory of Wave Propagation in Dispersive Systems (Jun. 13, 1967), pp. 6-25 <https://www.jstor.org/stable/2415780>

[22] Whitham, G.B., 2011. *Linear and nonlinear waves* (Vol. 42). John Wiley & Sons.